



Chapter 16

Additively Manufactured Component Characterization by Machine Learning from Resonance Inspection Techniques

Stephanie Gonzalez, Sierra D. Horangic, Joseph H. Lahmann, Timothy J. Ulrich, and Parisa Shokouhi

Abstract The lack of reliable, nondestructive part qualification for additively manufactured (AM) parts hinders their adoption in key industries of national interest such as aerospace and defense. Resonant ultrasound spectroscopy (RUS) is a relatively low-cost and nondestructive method for accurately determining material properties. In this work, we explored potential applications for using machine-learning techniques to computationally speed up RUS in deriving the material properties of AM parts, as well as identifying print quality of parts post-build. We performed mode identification on 226 cylinders manufactured via laser powder bed fusion (LPBF) from an A20X alloy. A lack of visual separation in the data lead to the use of statistical and dimensionality reduction techniques with the resonance peaks as well as examining the overlaid resonance spectra. We then performed classic RUS using a genetic algorithm to find the density, Young's modulus, and Poisson's ratio. By constraining these three parameters according to porosity relations relating all three material properties and training a random forest regression from finite element analysis simulations within a range of representative values, we could predict the material parameters with a lower mean RMS than compared to those values resulting from the less-constrained genetic algorithm.

Keywords Nondestructive Evaluation · RUS · Laser Doppler Vibrometry · Additive Manufacturing · Machine Learning

16.1 Introduction

Broader incorporation of additively manufactured (AM) parts in aerospace, automotive, and other industries could result in cost and lead time reductions, novel material development, unique designs, mass reduction through lightweight designs, and improved sustainment [1]. Despite its many benefits, AM is sensitive to a host of defects such as void or crack formation. Because there are various mechanisms within AM processes by which defects can be formed, nondestructive evaluation (NDE) methods are required to enact widespread use of AM parts in critical applications. X-ray radiography and computed tomography (CT) scans are currently used for high-resolution AM part inspection yet is often not fine enough to detect defects within individual layers [2]. Besides radiography and CT scans, methods such as magnetic particle testing, liquid penetrant testing, acoustic emission testing, eddy current testing, and visual testing have been employed as nondestructive testing techniques to varying degrees of success [3]. These methods have their own drawbacks including components needing to be cleaned before and after inspection, sensitivity being affected by the finish of a component, the ability to only inspect

S. Gonzalez

Department of Mechanical and Aerospace Engineering, University of Texas at El Paso, El Paso, TX, USA
e-mail: sgonzalez80@miners.utep.edu

S. D. Horangic

Department of Mechanical Engineering, Stanford University, Stanford, CA, USA

J. H. Lahmann

Department of Mechanical Engineering, Rose-Hulman Institute of Technology, Terre Haute, IN, USA

T. J. Ulrich (✉)

Los Alamos National Laboratory, Los Alamos, NM, USA
e-mail: tju@lanl.gov

P. Shokouhi

Pennsylvania State University, State College, PA, USA

non-porous surfaces, variability in magnetic permeability, and their effectiveness is restricted to conductive materials [3]. As such, there is a need for a reliable and more general nondestructive test for AM part inspection.

One promising technique is resonant ultrasound spectroscopy (RUS), which is a nondestructive evaluation technique that fits experimental modes to finite element (FE) calculated modes in order to obtain material properties like elements of the elastic moduli tensor. Elastic moduli influence the distribution of modes; the stiffer the sample is along one degree of freedom, the higher the frequency of the corresponding mode. The geometry of the sample influences the range of frequencies where the modes occur [4], and thus, the method can be used to infer changes in these properties from a standard reference point. RUS is of interest for AM part qualification due to these attributes. RUS has also been used to track the shifting of modes toward lower frequencies when a material undergoes phase transition. This is due to a relationship between RUS-derived elastic moduli and internal energy [5]. Previous attempts to determine material properties of complex geometries have consisted of mode matching and optimizing the fit between simulation and observed behavior. This process is referred to as inversion. The inversion process is a time-intensive, iterative minimization problem and largely relies heavily on accurate mode order matching for accuracy [6]. This project consisted of experimental modal testing on all samples, using various dimensionality reduction and statistical graphing techniques to look for visual separation in the data, and comparing the performance of classic RUS and a simulation-trained random forest regression model on calculating density, Poisson's ratio, and Young's modulus.

16.2 Background

Laser powder bed fusion (LPBF) selectively melts two-dimensional (2D) cross sections of the part to the previous layers of the part to successively create parts layer by layer. Laser processing parameters have a large effect on the densification and microstructure of materials used in LPBF technology. The high-energy density deposited into the metal powder by the laser leads to a full melting of the powder resulting in nearly or fully dense parts without the need for post-processing [7].

AM parts often have atypical geometry, which makes laser doppler vibrometry (LDV) an attractive option for modal testing since it is agnostic to shape. LDV covers broad frequencies and dynamic responses, which is not attainable by contact sensors. Results of a test previously conducted on rectangular parallelepiped specimens showed that LDV could detect modes that failed to be detected by contact approaches. In this case, non-contact detection exhibited superior sensitivity to detect frequencies as opposed to other approaches using contact sensors [8]. Implementing RUS using LDV has been recognized as an effective approach for material parameter estimation. However, RUS still suffers from the costly inversion process, which requires repeated simulations to be run while optimizing the model modes to the experimental. This makes using machine-learning (ML) models to learn this inversion an attractive idea.

ML techniques have an increasing popularity due to their ability to recognize subtle trends in complex datasets. Applying these methods to NDE methods has seen varied success across different materials and part inconsistencies. Chen et al. determined the elastic constants of a part made of piezoelectric material with high accuracy in as little as 150 ms. This was accomplished using 3 deep neural sub-networks which trained on a randomly created training set from FE analysis, only looking at a feature vector containing resonant frequencies [9]. From tests conducted by McGuigan et al., it was concluded that material property variance from the AM printing process played just as much of a role in defining the resonance spectra as their geometrical defects [3]. Oblaton et al. showed that resonant acoustic methods with purely experimental and labeled data, coupled with regularized linear discriminant analysis (RLDA), could result in 80% prediction accuracy of their test dataset [10]. Furthermore, calculating elastic constants can also be used to imply other information about the system. Ghosh et al. applied an ML algorithm to determine from raw spectral data the dimensionality of the order parameter for at lower temperatures [11].

16.3 Methodology

All testing was on a set of 226 cylinders of 10 mm diameter, Fig. 16.1, built with A20X across two build plates. Baseline parts were manufactured using laser settings of 200 W with a scan speed of 1000 mm/s and a hatch spacing of 0.1 mm. Altered parts were printed with one of these parameters varied up to $\pm 25\%$. These parameters can be combined into a volumetric energy term according to Eq. 16.1, where P is laser power, d is hatch spacing, s is scanning speed, and t is layer thickness.

Fig. 16.1 A sample test part, printed out of A20x with machine parameters engraved during printing on the top face



$$\text{Energy density} = \frac{P}{s \cdot d \cdot t} \quad (16.1)$$

Before modal testing, an eigenfrequency analysis was performed using Abaqus. This determined which modes could reasonably achieve mesh convergence, as well as provide a prediction for the modal shapes present. The parameter labeling on the top of the parts was defeated for simulation convergence, as it was found to result in negligible changes to the eigenfrequencies. To confirm mesh convergence, various modes were examined along decreasing mesh size. The most efficient mesh size was determined to be at 0.4 mm, where the first 30 modes were seen to be converging. Higher modes were excluded from consideration due to lack of convergence.

An experimental testing rig was designed and fabricated with the goal of minimally constraining the test part during testing, Fig. 16.2. Excitation was driven by a piezoelectric transducer and read with a point LDV at the crest of the part. The fixture created a point contact at 45° between the cylinder and the domed transducer and allowed for the excitation of as many modes as possible. A removable jig on the fixture allowed for a consistent placement of the cylinder and supportive foam served for minimal support to approximate a zero-boundary condition.

Frequency windows around modes of interest were identified, and the data collection excited the part across this spectrum, recording the response amplitude. Each window for each part resulted in a frequency response function (FRF) such as Fig. 16.3.

Mode matching (as well as further validation of the simulation) was done by matching 2D modal shapes. Test parts were excited at a mode, then scanned across the surface with a 2-D LDV for all the modes identified as detectable in our setup. This identification is represented in Table 16.1.

Simulations served a second purpose beyond determining experimental windows. It is also used in the creation of a synthetic dataset for training regression models. Prior work by Ramakrishnan provides the basis for calculating Young's modulus and Poisson's ratio from density, as established by Eqs. 16.2, 16.3, and 16.4 [12]. So, a synthetic dataset was created by varying only the density of the part.

$$P = 1 - \frac{\rho}{\rho_0} \quad (16.2)$$

Table 16.1 The correlation between the simulated mode shapes and experimentally observed mode shapes

Mode feature #	1	2	3	4	5	6	7	8	9	10	
Mode #	1	2	4	9	10	13	14	15	22	23	
Observed shape											
Simulation predicted shape											

Note: mode 23 appears to be mismatched; this mode was found to be sensitive to small variations in material properties

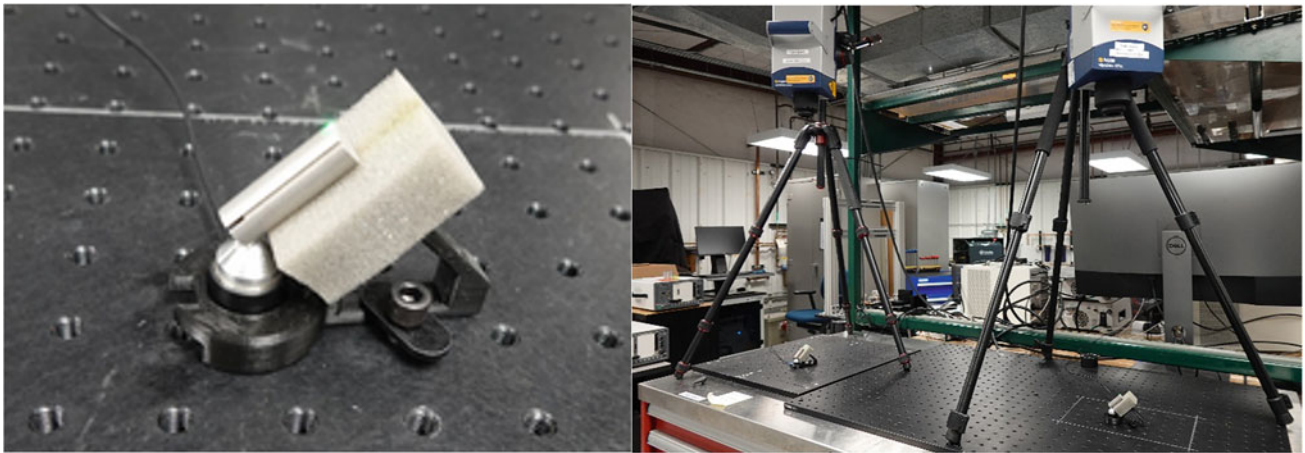


Fig. 16.2 Left: Excitation rig loaded with a part, showing orientation and direction of LDV. Right: two experimental testing rigs shown side by side

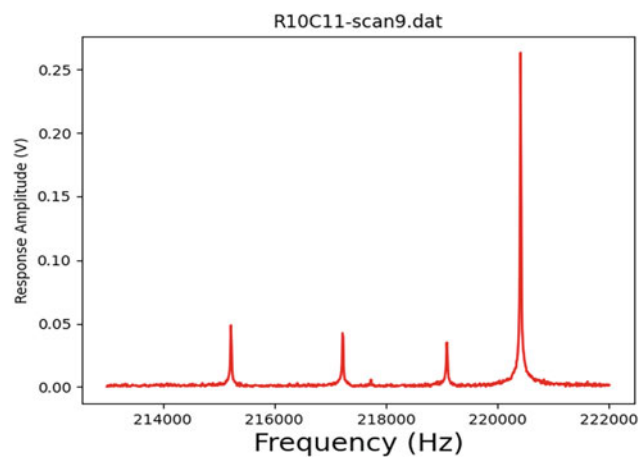


Fig. 16.3 A sample experimental FRF showing a dense nodal region

$$E = E_0 \frac{(1 - P)^2}{1 + (2 - 3\nu) P} \quad (16.3)$$

$$\nu = \frac{4\nu_0 + 3P - 7\nu_0 P}{1 + 2P - 3\nu_0 P} \quad (16.4)$$

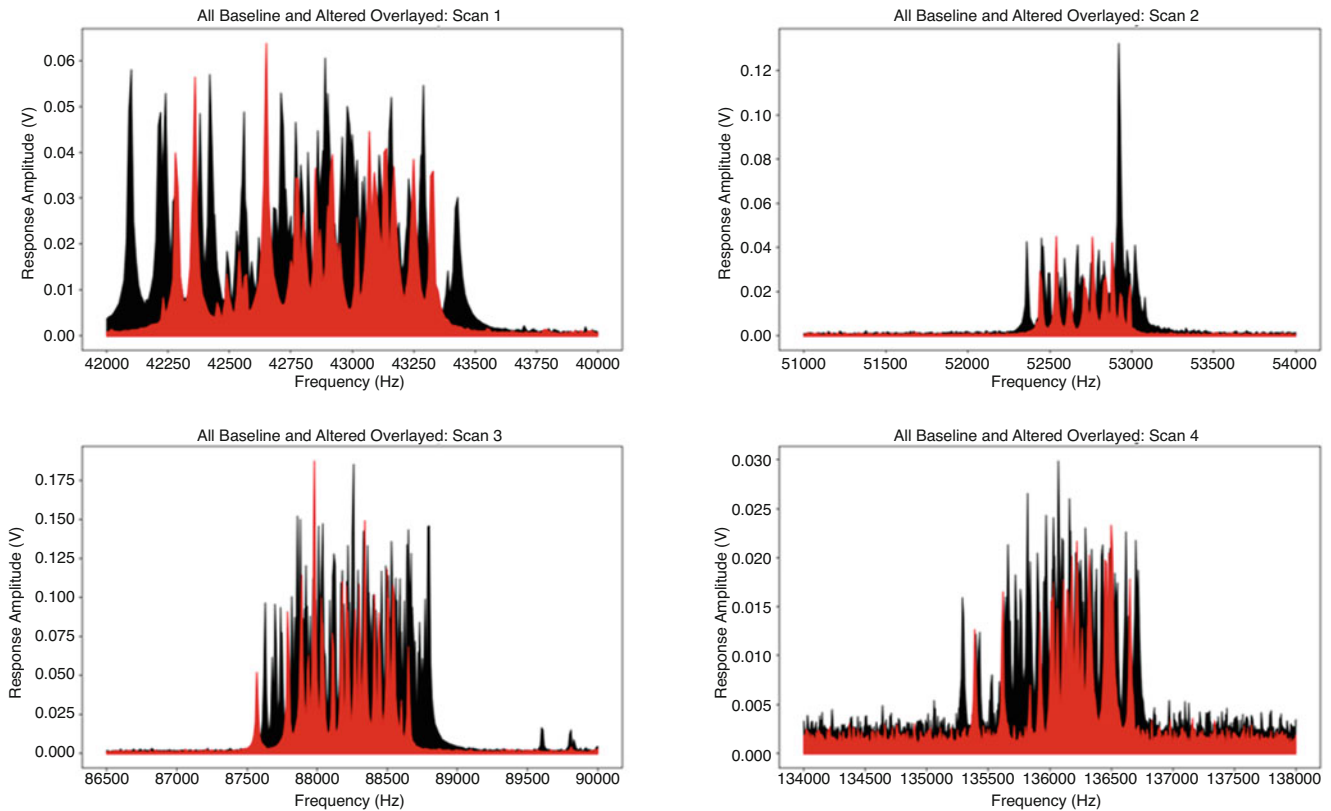
16.4 Analysis

Variability of the testing rig was evaluated by testing a single part repeatedly, removing and remounting from the test rig six times. Standard deviations for nearly all modes in this test were all under 10 Hz. One mode saw a standard deviation of nearly 50 Hz and was subsequently excluded from further analysis due to excessive noise. Drift was also evaluated by leaving the same part on the test rig overnight, during which 136 scans were run for each of the frequency ranges of interest. The calculated standard deviation of the modal frequencies is shown in Table 16.2. This is likely due to temperature variation, which could be confirmed in the future by tracking temperature.

To understand the differences between the baseline and altered parts, the scans for each window were overlaid as shown in Fig. 16.4. From this, we can see that the spectra for the altered parts lie solidly within the reasonable range of response for the baseline. Looking at the statistical distributions, there is no clear separation either in comparing the frequency distribution for each mode (Fig. 16.5) or the peak width distribution for each mode (Fig. 16.6).

Table 16.2 Standard deviation of the modal frequencies as measured across all modal scans

Mode	1	2	3	4	5	6	7	8	9	10
Modal frequency	43.1 kHz	43.4 kHz	88.8 kHz	136.5 kHz	143.8 kHz	172.2 kHz	178.1 kHz	184.4 kHz	220.7 kHz	229.1 kHz
Standard deviation	7.7 Hz	8.1 Hz	14.8 Hz	23.9 Hz	24.6 Hz	29.8 Hz	31.7 Hz	32.9 Hz	38.7 Hz	41.2 Hz

**Fig. 16.4** Overlaid FRF scans of baseline (black) and altered (red) parts, displaying how the range of responses of the altered parts is firmly within the range of the baseline

Various dimensionality reduction techniques were also applied to the data to look for insight for separation, including linear principal component analysis (PCA), kernel PCA (cosine, radial basis function, and polynomial kernels), and manifold learning techniques (isomap, local linear embedding, and spectral embedding). These were all applied on various combinations of modal frequency, amplitude, and peak width. For all, the first three components (or two in the case of manifold learning) were plotted and examined visually, with the true labels of the build parameters (in the form of volumetric energy density) coloring data points. In all cases, there was no clear separation in the data between the baseline and altered parts.

Density-based spatial clustering of applications with noise (DBSCAN) clustering was used to delineate clusters when visualizing datasets [13]. Figure 16.7 shows clustering of the parts based on their damping fraction for all seven modes. One dense, distinct cluster, as well as another comprised of outliers can be seen. Visualizing these results along the first three damping components clearly showed a physical correlation between the yellow cluster and internal damping—the cluster appears near the corner with the lowest damping fractions, and the outliers have larger damping fractions for at least one of their modes. This could indicate that damping could be a valuable feature to track during any component characterization.

To look at the performance of a ML model learning the RUS inversion, a random forest regression was implemented by training on the synthetic dataset created according to Ramakrishnan's correlations. Table 16.3 shows the gap between the predicted values by RUS and the regression. The average root-mean-square RMS error from the frequency matching of all parts was found to be 0.92% for the random forest regression as compared to 1.51% for standard RUS. This performance boost with the random forest regression is likely due to the standard RUS inversion being under constrained and finding a local minimum.

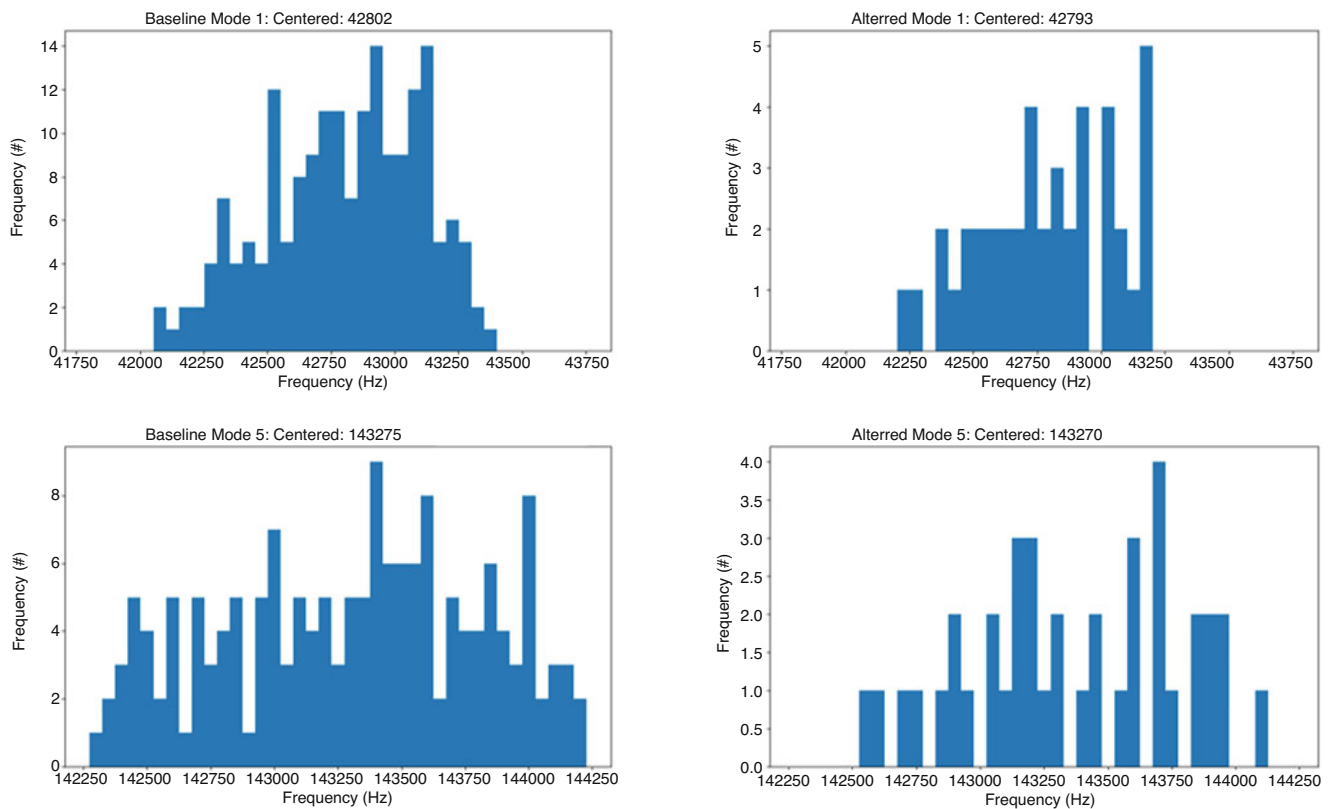


Fig. 16.5 Sample modal distributions indicate the similarity between baseline and altered results

Table 16.3 The sample comparison between RUS and random forest regression for one baseline part (R3 C10) in calculating the material properties

	Predicted density	Predicted elastic modulus (MPa)	Predicted Poisson’s ratio
Regression	2.77 g/mm ³	77,800	0.339
RUS	2.78 g/mm ³	63,470	0.316

16.5 Conclusion

The experimental results indicate that it is likely the test parts used are all within the relative bounds of acceptable printing parameters. For the methods utilized, there was no detectable shift in the material properties correlated with the build parameters, although DBSCAN clustering indicates the possibility of a clumping of parts along their damping characteristics. Plotting after dimensionality reduction, statistical distributions, and overlaid raw data can give insight to the feature selection process when designing a model for NDE.

The experimental results further indicate this random forest regression outperforms our standard RUS inversion in prediction accuracy. This ML regression has a high initial computational cost, with subsequent calculations becoming negligible after the model is trained. Conventional RUS has a relatively constant need to perform many simulations for a single regression. Given a high volume of parts, this ML regression would easily outstrip conventional RUS. Ultimately, this work indicates the potential of training ML regressions using constrained training data.

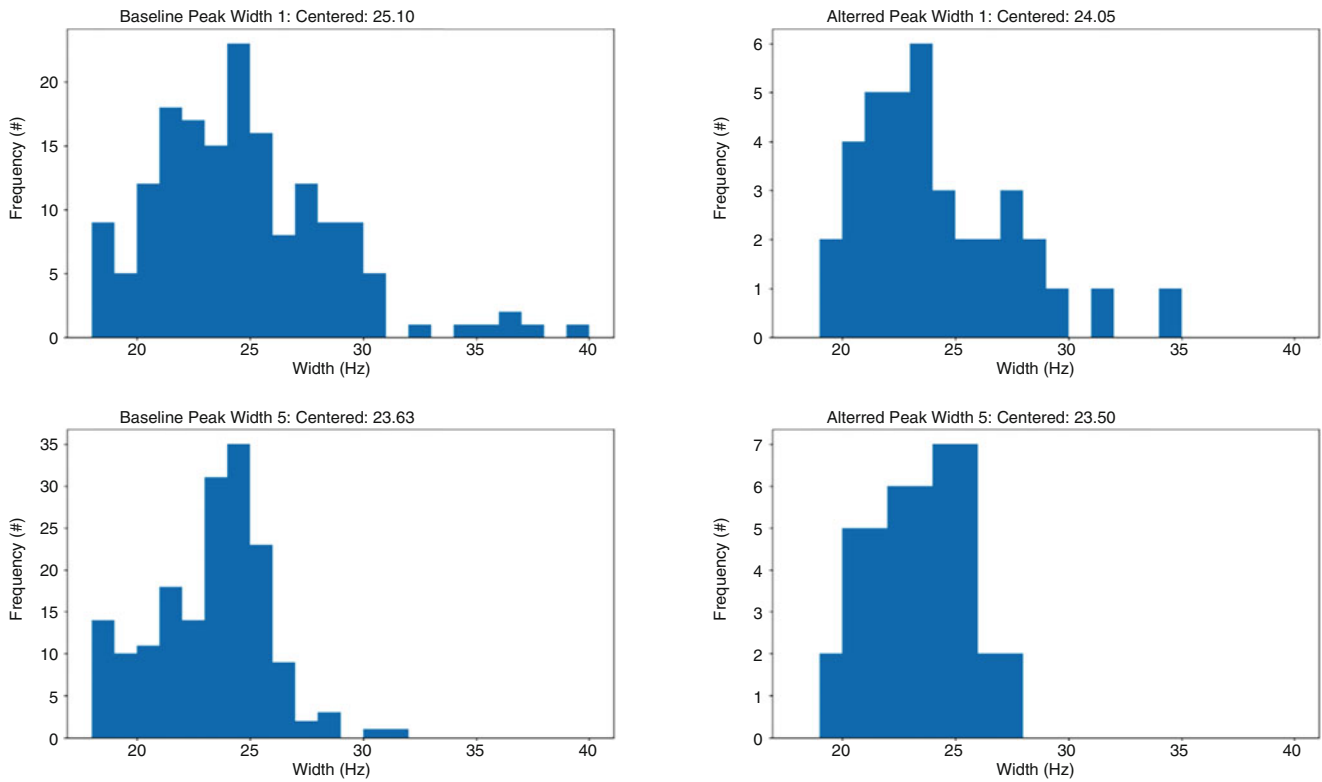


Fig. 16.6 Sample peak width distributions indicate the similarity between baseline and altered results

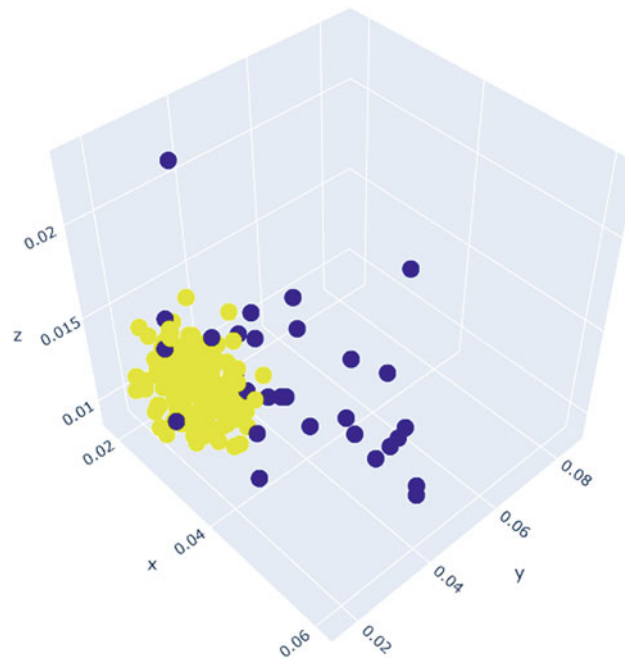


Fig. 16.7 DBSCAN labeling based on the damping for all modes

Acknowledgments This research was funded by Los Alamos National Laboratory (LANL) through the Engineering Institute’s Los Alamos Dynamics Summer School. The Engineering Institute is a research and education collaboration between LANL and the University of California San Diego’s Jacobs School of Engineering. This collaboration seeks to promote multidisciplinary engineering research that develops and integrates advanced predictive modeling, novel sensing systems, and new developments in information technology to address LANL mission relevant problems.

Furthermore, we would like to thank Mr. Luke Beardslee for authoring and supplying the RUS code used to calculate inversions on all test parts. We would also like to thank Dr. Adam J. Wachtor for his guidance, editing suggestions, and support during the entire course of research.

References

1. Milner, B., Gradl, P., et al.: Metal additive manufacturing in aerospace: a review. *Mater. Des.* **209**, 110008 (2021). <https://doi.org/10.1016/j.matdes.2021.110008>. ISSN 0264-1275
2. Edgar, S.: Non-destructive testing of additive manufactured parts. 2020. <https://www.azom.com/article.aspx?ArticleID=19038>
3. McGuigan, S., Arguelles, A.P., Obaton, A.-F., Donmez, A.M., Riviere, J., Shokouhi, P.: Resonant ultrasound spectroscopy for quality control of geometrically complex additively manufactured components. In: *Additive Manufacturing*, vol. 39, p. 101808. Elsevier BV (2021). <https://doi.org/10.1016/j.addma.2020.101808>
4. Zadler, B.J., Le Rousseau, J.H., Scales, J.A. and Smith, M.L.: Resonant ultrasound spectroscopy: theory and application. *Geophysical Journal International*, **156**(1), pp.154–169. (2004)
5. Balakirev, F.F., et al.: Resonant ultrasound spectroscopy: the essential toolbox. *Rev. Sci. Instrum.* **90**(12), 121401 (2019)
6. Beardslee, L., Remillieux, M., Ulrich, T.J.: Determining material properties of components with complex shapes using resonant ultrasound spectroscopy. *Appl. Acoust.* <https://doi.org/10.1016/j.apacoust.2021.108014>
7. Cobbinah, P., Nzeukou, R., Onawale, O., Matizamhuka, W.: Laser powder bed fusion of potential superalloys: a review. *Metals*. **11**, 58 (2020). <https://doi.org/10.3390/met11010058>
8. AIP Conf.Proc. **1949**, 170002 (2018); Published Online: 20 April 2018
9. Chen, Z., Miao, X., Li, S., Zheng, Y., Xiong, K., Qin, P., Han, T.: Data fusion method and probabilistic pairing approach in elastic constants measurement by resonance ultrasound spectroscopy. In: *IEEE Transactions on Instrumentation and Measurement*, vol. 69, Issue 6, pp. 2948–2958. Institute of Electrical and Electronics Engineers (IEEE) (2020). <https://doi.org/10.1109/tim.2019.2925409>
10. Obaton, A.-F., Wang, Y., Butsch, B., Huang, Q.: A non-destructive resonant acoustic testing and defect classification of additively manufactured lattice structures. In: *Welding in the World*, vol. 65, Issue 3, pp. 361–371. Springer Science and Business Media LLC (2021). <https://doi.org/10.1007/s40194-020-01034-7>
11. Ghosh, S., Matty, M., Baumbach, R., Bauer, E.D., Modic, K.A., Shekhter, A., Mydosh, J.A., Kim, E.-A., Ramshaw, B.J.: One-component order parameter in URu₂Si₂ uncovered by resonant ultrasound spectroscopy and machine learning. In: *Science Advances*, vol. 6, Issue 10. American Association for the Advancement of Science (AAAS) (2020). <https://doi.org/10.1126/sciadv.aaz4074>
12. Choren, J.A., Heinrich, S.M., Silver-Thorn, M.B.: Young's modulus and volume porosity relationships for additive manufacturing applications. *J. Mater. Sci.* **48**(15), 5103–5112 (2013). <https://doi.org/10.1007/s10853-013-7237-5>
13. Ester, M., Kriegel, H.-P., Sander, J., Xu, X.: A density-based algorithm for discovering clusters in large spatial databases with noise. www.aaii.org (1996)